



## Search for Pair Production of Top Squarks Decaying to a $\tau$ Lepton and a $b$ Quark

The CDF Collaboration  
URL <http://www-cdf.fnal.gov>  
(Dated: January 30, 2005)

We present the results of a search for pair production of scalar top quarks ( $\tilde{t}_1$ ) in an  $R$ -parity violating supersymmetry scenario in  $200 \text{ pb}^{-1}$  of  $p\bar{p}$  collisions at  $\sqrt{s} = 1.96 \text{ TeV}$  collected by the Collider Detector at Fermilab. In this case each  $\tilde{t}_1$  decays into a  $\tau$  lepton and a  $b$  quark. The final state is either an electron or a muon ( $\ell = e$  or  $\mu$ ) from the  $\tau \rightarrow \ell\nu_\ell\nu_\tau$  decay, as well as a hadronically decaying  $\tau$  lepton, and two or more jets. Five candidate events pass our final selection criteria, which is consistent with the standard model expectation of  $4.8 \pm 0.7$  events. We set a 95% confidence level lower limit on the  $\tilde{t}_1$  mass,  $m(\tilde{t}_1)$ , at  $134 \text{ GeV}/c^2$  for  $\mathcal{B}(\tilde{t}_1 \rightarrow \tau b) = 1$  with the next-to-leading order calculation of the cross section using CTEQ6M parton distribution functions (PDFs) and a renormalization scale of  $Q^2 = \sqrt{m(\tilde{t}_1)^2 + p_T^2}$ . If we include theoretical uncertainties in the cross section calculation due to the renormalization scales and PDFs, a conservative limit of  $m(\tilde{t}_1) > 129 \text{ GeV}/c^2$  is obtained. These limits are also fully applicable to the case of the third generation scalar leptoquark ( $LQ_3$ ) assuming a 100% branching ratio for the  $LQ_3 \rightarrow \tau b$  decay mode.

## I. INTRODUCTION

Various supersymmetric (SUSY) models [1] predict that the first two generations of SUSY partners of the quarks and the leptons (squarks and sleptons) are approximately mass degenerate. However, the mass of the lightest top squark ( $\tilde{t}_1$  or ‘stop’) can be relatively light due to a large mixing between the interaction eigenstates,  $\tilde{t}_L$  and  $\tilde{t}_R$ . This mixing depends in part on the top Yukawa coupling which is largely due to the heavy top quark mass, and it is possible that  $\tilde{t}_1$  is lighter than the top quark [2]. Within a framework of  $R_p$  violating ( $\mathcal{R}_p$ ) SUSY [3], each  $\tilde{t}_1$  decays to a tau ( $\tau$ ) lepton and a bottom ( $b$ ) quark with a branching ratio,  $\mathcal{B}$ , which depends on the coupling constants of the particular model.

In  $p\bar{p}$  collisions at  $\sqrt{s} = 1.96$  TeV at the Fermilab Tevatron, stop pairs might be produced strongly via  $R_p$ -conserving processes through  $gg$  fusion and  $q\bar{q}$  annihilation. In this paper we describe a search for  $\tilde{t}_1\tilde{t}_1 \rightarrow \tau\tau b\bar{b}$  with the CDF II detector [4] in a final state of either an electron or a muon ( $\ell = e$  or  $\mu$ ) from the  $\tau \rightarrow \ell\nu\ell\nu_\tau$  ( $\tau_\ell$ ) decay, as well as a hadronically decaying tau ( $\tau_h$ ) lepton, and two or more jets. We assume  $\mathcal{B}(\tilde{t}_1 \rightarrow \tau b) = 1$ .

## II. DATA SAMPLE AND EVENT SELECTION

The analysis begins with a data sample collected by inclusive lepton plus track triggers [5] that require an electron candidate with calorimeter cluster  $E_T > 8$  GeV ( $|\eta| < 1.1$  in CEM) or a muon candidate with track momentum  $p_T > 8$  GeV/ $c$  ( $|\eta| < 0.6$  in CMUP;  $0.6 < |\eta| < 1$  in CMX), and an additional XFT track with  $p_T > 5$  GeV/ $c$  [6, 7]. The integrated luminosity of the data sample for CEM and CMUP (CMX) is  $197 \text{ pb}^{-1}$  ( $178 \text{ pb}^{-1}$ ).

We select events by identifying at least one lepton with  $p_T^\ell > 10$  GeV/ $c$  for the CEM electron, CMUP or CMX muon) and at least one  $\tau_h$  candidate with  $p_T^\tau > 15$  GeV/ $c$  in the fiducial region of the detector. Jets are identified with a fixed-cone of  $\Delta R = 0.4$  in  $|\eta| < 2.4$  and required to have  $E_T > 15$  GeV and separated from any of  $e$ ,  $\mu$ , and  $\tau_h$  by  $\Delta R > 0.8$ .

We then apply for a series of event topology cuts designed to improve the sensitivity of the search, where the dominant standard model (SM) backgrounds are QCD events ( $b\bar{b}$ ,  $\gamma + \text{jet}$ ) and vector bosons with multiple jets. The events are removed if (a) the primary electron is from photon conversion or the primary muon is a cosmic ray muon ( $|\phi_\mu - \phi_\tau^{\text{seedtrack}} - \pi| < 0.1$  for  $N_{\text{jet}} = 0$ ); (b) the invariant mass of the primary electron and a loosely-identified second electron candidate is  $76 < m_{e^+e^-} < 106$  GeV/ $c^2$ ; (c) the  $e$ - $\tau_h$  system satisfies the three criteria:  $(f^{\text{EM}(\tau_h)} - 0.4)^2 / (0.4)^2 + (\Delta\phi_{e\tau} - 1.5)^2 / (1.5)^2 \geq 1$  if  $\Delta\phi_{e\tau} > 1.5$  and  $m_T(e, \cancel{E}_T) \equiv \sqrt{2 p_T^e \cancel{E}_T (1 - \cos \Delta\Phi)} > 35$  GeV/ $c^2$ , where  $f^{\text{EM}(\tau_h)}$  is a fraction of the EM energy to the total  $\tau_h$  energy cluster and  $\Delta\Phi$  is an azimuthal angle between  $e$  and  $\cancel{E}_T$ ; (d) the invariant mass of the primary muon and a loosely-identified second muon candidate is  $66 < m_{\mu^+\mu^-} < 111$  GeV/ $c^2$ ; (e)  $S_T \equiv p_T^\ell + p_T^{\tau_h} + \cancel{E}_T < 85$  GeV. Cut (c) is to remove the events in a region of high transverse mass of electron and missing transverse energy where one of two electron legs in  $Z \rightarrow e^+e^-$  decay is not well measured in the detector and mis-identified as a  $\tau_h$ . Cut (e) is to suppress the QCD and  $Z \rightarrow \tau^+\tau^-$  events [8] and re-optimized for this analysis.

We define the primary signal region (A<sub>2</sub>) with (f)  $N_{\text{jet}} \geq 2$  and (g)  $m_T(\ell, \cancel{E}_T) < 35$  GeV/ $c^2$  along with other five regions as defined in Table I. We estimate the geometrical/kinematical acceptances ( $A_{\text{geom/kine}}$ ), efficiencies for identification (ID) and isolation (ISO) cuts ( $\epsilon_{\text{ID}}$  and  $\epsilon_{\text{ISO}}$ ), lepton and XFT track trigger efficiencies ( $\epsilon_{\text{trig}}^\ell$  and  $\epsilon_{\text{trig}}^{\text{XFT}}$ ), a total acceptance for event topological cuts ( $\epsilon_{\text{topo}}$ ), using PYTHIA [9] with the GEANT-based [10] CDF detector simulation or data. Our nominal choice of parton distribution functions (PDFs) and a renormalization scale ( $Q^2$ ) is CTEQ6 [11] and  $Q^2 = \sqrt{m(\tilde{t}_1)^2 + p_T^2}$ . The estimated numbers are summarized in Table II for  $\tilde{t}_1\tilde{t}_1 (\rightarrow \tau_\ell\tau_h b\bar{b})$  events ( $m(\tilde{t}_1) = 130$  GeV/ $c^2$ ) in region A<sub>2</sub>. Figure 1 is the total event acceptance ( $\alpha \equiv A_{\text{geom/kine}} \cdot \epsilon_{\text{ID}} \cdot \epsilon_{\text{ISO}} \cdot \epsilon_{\text{trig}} \cdot \epsilon_{\text{topo}}$ ) as a function of  $m(\tilde{t}_1)$ . Here  $\epsilon_{\text{ID}} = \epsilon_{\text{ID}}^\ell \cdot \epsilon_{\text{ID}}^{\tau_h}$ ,  $\epsilon_{\text{ISO}} = \epsilon_{\text{ISO}}^\ell \cdot \epsilon_{\text{ISO}}^{\tau_h}$ ,  $\epsilon_{\text{trig}} = \epsilon_{\text{trig}}^\ell \cdot \epsilon_{\text{trig}}^{\text{XFT}}$ .

It should be noted that to avoid biasing our result, a ‘blind’ analysis technique is employed, where the data in region A<sub>2</sub> is ‘blinded’ until we fully optimize the event selection criteria for signal events and estimate the signal event acceptance and the background (BG) events in each of six regions.

## III. BACKGROUNDS

The SM backgrounds are (i) events with true  $\ell\tau_h$  pair from  $Z^0/\gamma^* (\rightarrow \tau^+\tau^-) + \text{jets}$ ,  $t\bar{t}$  and diboson ( $W^+W^-$ ,  $W^\pm Z^0$ ,  $Z^0 Z^0$ ) production; (ii) events with fake  $\ell\tau_h$  combination from  $W + \text{jet}$ ,  $Z^0/\gamma^* (\rightarrow \ell^+\ell^-) + \text{jets}$ , and QCD events. We first estimate all SM background events excluding  $W + \text{jet}$  events.  $Z^0/\gamma^* (\rightarrow \tau^+\tau^-) + \text{jets}$  are estimated using PYTHIA

TABLE I: Definition of six regions in the  $m_T$ - $N_{\text{jet}}$  plane, where  $A_2$  is the primary signal region. Regions  $A_0$ ,  $B_0$ ,  $A_2$  and  $B_2$  are used in setting final limit, regions  $A_1$  and  $B_1$  will be used as control regions.

	$m_T < 35 \text{ GeV}/c^2$	$m_T > 35 \text{ GeV}/c^2$
$N_{\text{jet}} \geq 2$	$A_2$	$B_2$
$N_{\text{jet}} = 1$	$A_1$	$B_1$
$N_{\text{jet}} = 0$	$A_0$	$B_0$

TABLE II: Acceptances and efficiencies (in %) for  $\tilde{t}_1\bar{\tilde{t}}_1 \rightarrow \tau_\ell\tau_h b\bar{b}$  in region  $A_2$  in the case of  $m(\tilde{t}_1) = 130 \text{ GeV}/c^2$ . Two systematical uncertainties are shown for  $A_{\text{geom/kine}}$ ,  $\epsilon_{\text{ID}}$ ,  $\epsilon_{\text{ISO}}$ , and  $\epsilon_{\text{trig}}$ . The first is due to the statistical uncertainty since it is determined by MC or control data samples; the second is the systematic uncertainty in the CDF detector simulation program.

	$e + \tau$	$\mu^{\text{CMUP}} + \tau$	$\mu^{\text{CMX}} + \tau$
$A_{\text{geom/kine}}$ Geometrical/kinematical acceptance for $\ell$ and $\tau_h$ with $\Delta R$ cut	$14.7 \pm 0.1 \pm 0.2$	$9.35 \pm 0.12 \pm 0.18$	$3.35 \pm 0.08 \pm 0.05$
$\epsilon_{\text{ID}}$ Lepton identification efficiency	$85.2 \pm 0.4 \pm 0.9$	$85.7 \pm 0.4 \pm 4.0$	$88.7 \pm 0.8 \pm 1.0$
Tau identification efficiency	$71.7 \pm 0.6 \pm 2.2$	$72.3 \pm 0.8 \pm 2.2$	$71.5 \pm 1.3 \pm 2.1$
$\epsilon_{\text{ISO}}$ Lepton isolation efficiency	$79.0 \pm 0.5 \pm 2.4$	$82.5 \pm 0.5 \pm 2.5$	$84.5 \pm 0.9 \pm 2.5$
Tau isolation efficiency	$68.9 \pm 0.8 \pm 2.1$	$70.6 \pm 1.0 \pm 2.1$	$70.2 \pm 1.8 \pm 2.1$
$\epsilon_{\text{trig}}$ Lepton trigger efficiency	$97.1 \pm 0.2 \pm 1.0$	$95.5 \pm 0.3 \pm 1.0$	$95.4 \pm 0.6 \pm 1.0$
XFT-track trigger efficiency		$\leftarrow 96.2 \pm 0.5 \pm 1.0 \rightarrow$	
$\epsilon_{\text{topo}}$ Total acceptance for event topology	$45.1 \pm 1.0$	$52.0 \pm 1.2$	$48.1 \pm 2.1$
$\alpha$ : Total Event Acceptance	$2.06 \pm 0.06$	$1.60 \pm 0.05$	$0.56 \pm 0.03$

[9] and the GEANT-based [10] CDF detector simulation with the correction factors for the  $N_{\text{jet}}$  distribution obtained from  $Z^0 \rightarrow \ell^+ \ell^-$  data. The QCD events are estimated using the lepton ISO distribution using a data sample of non-isolated leptons. The contribution from  $Z^0/\gamma^*(\rightarrow \ell^+ \ell^-) + \text{jets}$ ,  $t\bar{t}$ ,  $W^+W^-$ ,  $W^\pm Z^0$ , and  $Z^0 Z^0$  production is estimated using with PYTHIA [9] and the detector simulation program. The cross sections for  $t\bar{t}$ ,  $W^+W^-$ ,  $W^\pm Z^0$ , and  $Z^0 Z^0$  production are normalized to next-to-leading order (NLO) calculations of 6.7, 12.4, 3.78, and 1.4 pb, respectively.

In Table III we show the number of events observed in data, along with the expected number of SM events excluding the  $W + \text{jet}$  events. It should be noted that the number of events in data in region  $A_2$  (shown in the boldface numbers) are only known after all event selection cuts are finalized and the SM backgrounds are estimated. The  $N_{\text{jet}}$  distribution for a data sample of events in  $m_T < 35 \text{ GeV}/c^2$  (regions  $A_0$ ,  $A_1$ , and  $A_2$ ) is shown in Figure 2, where the  $W + \text{jet}$  contribution is negligible. There is a good agreement between the data and the SM prediction in each jet multiplicity. A total of five events found in region  $A_2$  are consistent with the SM expectation.

We note that large discrepancies between ‘Observed’ and ‘BG’ in regions  $B_0$  and  $B_1$  are expected from the  $W + \text{jet}$  contribution. We estimate the  $W + \text{jet}$  contributions in  $A_2$  and  $B_2$  as  $N^{W+j}(A_2) = N^{W+j}(A_0) \cdot \mathcal{R}_A$  and  $N^{W+j}(B_2) = N^{W+j}(B_0) \cdot \mathcal{R}_B$ , where  $\mathcal{R}_A \sim \mathcal{R}_B$ . The values of  $\mathcal{R}$  for  $m_T < 35 \text{ GeV}/c^2$  and  $m_T > 35 \text{ GeV}/c^2$  are estimated with PYTHIA plus the detector simulation. We find the ratio of two  $\mathcal{R}$  values to be  $1.0 \pm 0.5$ . The large uncertainty does not affect in setting the mass limit, because the  $W + \text{jet}$  contributions in regions  $A_2$  and  $B_2$  are negligible.

#### IV. SYSTEMATIC UNCERTAINTIES

The sources of systematic uncertainties for the acceptance for  $\tilde{t}_1\bar{\tilde{t}}_1 \rightarrow \tau_\ell\tau_h b\bar{b}$  are uncertainties from (a) PDFs, (b) initial and final state radiation (ISR and FSR), (c) jet energy scale, (d)  $\cancel{E}_T$  simulation, (e) identification and isolation efficiencies for  $e$ ,  $\mu$ , and  $\tau_h$ , (f) geometrical and kinematical acceptance in the detector simulation. The combined systematic uncertainty for the electron (muon) channel varies from 8.3% (8.8%) for the stop mass of  $m(\tilde{t}_1) = 100 \text{ GeV}/c^2$  and 6.7% (6.9%) for  $160 \text{ GeV}/c^2$ .

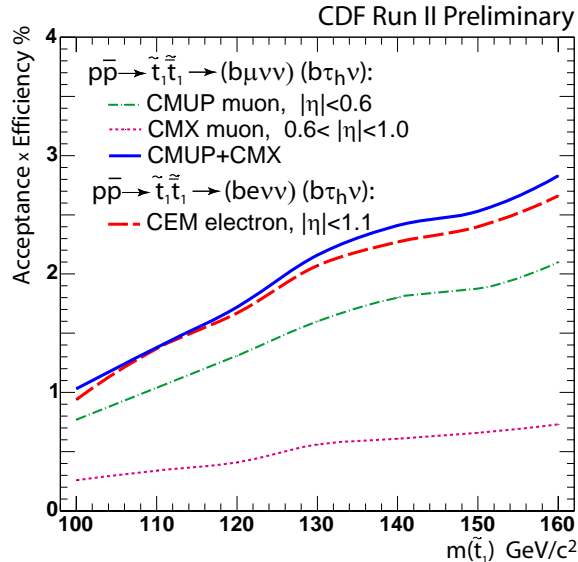


FIG. 1: Total event acceptance as a function of the stop mass,  $m(\tilde{t}_1)$ , for different lepton plus track triggers.

TABLE III: Number of events observed in data, along with the expected number of SM background (BG) events excluding the  $W + \text{jet}$  contribution. The data in region  $A_2$  is ‘blinded’ until we fully optimize the event selection criteria for signal events and estimate the signal event acceptance and the number of BG events in each of six regions.

Region	$e + \tau$ Channel		$\mu + \tau$ Channel	
	Observed	BG (excluding $W + \text{jet}$ )	Observed	BG (excluding $W + \text{jet}$ )
$A_2$	<b>2</b>	$2.60^{+0.58}_{-0.53}$	<b>3</b>	$2.21^{+0.50}_{-0.30}$
$B_2$	3	$2.94^{+0.80}_{-0.73}$	4	$2.60^{+0.46}_{-0.32}$
$A_1$	7	$6.58^{+0.64}_{-0.55}$	5	$5.58^{+0.77}_{-0.55}$
$B_1$	16	$3.29^{+0.62}_{-0.48}$	12	$2.34^{+0.50}_{-0.31}$
$A_0$	22	$25.90^{+1.29}_{-1.20}$	5	$5.56^{+0.57}_{-0.40}$
$B_0$	37	$4.19^{+0.57}_{-0.43}$	48	$6.28^{+0.77}_{-0.66}$

## V. CROSS SECTION AND MASS LIMITS

With no excess in region  $A_2$ , a 95% confidence level (C.L.) limit on the  $\tilde{t}_1\bar{\tilde{t}}_1$  production cross section ( $\sigma$ ) is calculated. We define a likelihood function using Poisson statistics as a function of  $\sigma$  using:

- Number of observed events in each of the regions  $A_2$ ,  $B_2$ ,  $A_0$ , and  $B_1$ ;
- Number of expected events in each region,  $N_i = \sigma \cdot \mathcal{B}(\tau\tau \rightarrow \tau_\ell\tau_h) \cdot \int \mathcal{L} dt \cdot \alpha_i + N_i^{\text{BG}} + N_i^{W+j}$ , where  $N_i^{\text{BG}}$  includes all SM backgrounds excluding  $W + \text{jet}$  events,  $\alpha_i$  is the total event acceptance for signal in region  $i$  (note that  $\alpha_i$  is negligibly small for regions  $A_0$  and  $B_0$ );
- $\mathcal{R}_B/\mathcal{R}_A = 1.0 \pm 0.5$ , taking the absolute rate of the  $W + \text{jet}$  events as a nuisance parameter.

The likelihood function is a probability of observing the number of events found in data given the signal cross section. Electron and muon channels are treated as two separate measurements, taking into account correlated systematic uncertainties.

Table IV shows 95% C.L. upper limits on the cross section as a function of  $m(\tilde{t}_1)$ . The 95% C.L. limit curve (thick solid line in red) is shown in Fig. 3, comparing to the NLO cross sections [12] for our nominal choice of CTEQ6M PDFs [11] and a renormalization scale of  $Q^2 = \sqrt{m(\tilde{t}_1)^2 + p_T^2}$  (blue, solid), while two dashed lines with  $\pm 18\%$  uncertainties due to the choice of  $Q^2$  (varying the scale from its nominal value by a factor of two or a half) and PDFs. We find

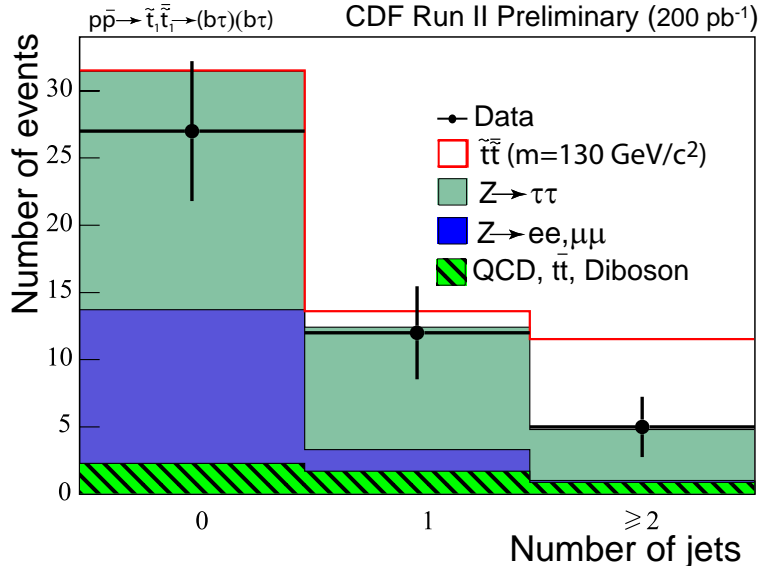


FIG. 2: Distribution of  $N_{\text{jet}}$  for events in  $m_T < 35 \text{ GeV}/c^2$ , compared to the expectations from SM background and  $\tilde{t}_1\bar{\tilde{t}}_1$  ( $m(\tilde{t}_1) = 130 \text{ GeV}/c^2$ ) events.

TABLE IV: 95% C.L. upper limit on the  $\tilde{t}_1\bar{\tilde{t}}_1$  production cross section (in pb) as a function of  $m(\tilde{t}_1)$  with our nominal choice of CTEQ6M PDFs [11] and a renormalization scale of  $\sqrt{m(\tilde{t}_1)^2 + p_T^2}$ . We assume  $\mathcal{B}(\tilde{t}_1\bar{\tilde{t}}_1 \rightarrow \tau\tau b\bar{b}) = 1$ .

		$m(\tilde{t}_1) \text{ (GeV}/c^2\text{)}$						
$N_{\text{evt}}^{e+\tau_h}$	$N_{\text{evt}}^{\mu+\tau_h}$	100	110	120	130	140	150	160
2	3	6.75	4.75	3.75	3.05	2.75	2.65	2.35

$m(\tilde{t}_1) > 134 \text{ GeV}/c^2$  for the nominal choice and a conservative mass limit of  $m(\tilde{t}_1) > 129 \text{ GeV}/c^2$ . The previously published limit of  $m(\tilde{t}_1) > 122 \text{ GeV}/c^2$  [8] should be compared to  $134 \text{ GeV}/c^2$ .

It should be noted that the stop pair production process is very similar to the pair production of the third generation scalar leptoquark. The cross sections become identical in the limit of heavy gluino. Thus, the same mass limit is applicable.

## VI. CONCLUSIONS

We have searched for  $\tilde{t}_1\bar{\tilde{t}}_1$  production in the final state of a lepton, a  $\tau_h$  and two jets using  $200 \text{ pb}^{-1}$  of  $p\bar{p}$  collision data at  $\sqrt{s} = 1.96 \text{ TeV}$ . The final state would be expected within a  $\mathcal{R}_p$  SUSY scenario of  $\tilde{t}_1 \rightarrow \tau b$ . With an observation of five events that was consistent with the SM background expectation, we set a 95% C.L. lower limit on the  $\tilde{t}_1$  mass to be  $129 \text{ GeV}/c^2$  taking into account the theoretical uncertainties on the NLO cross section due to the uncertainties on  $Q^2$  and PDFs.

## Acknowledgments

We thank the Fermilab staff and the technical staffs of the participating institutions for their vital contributions. This work was supported by the U.S. Department of Energy and National Science Foundation; the Italian Istituto Nazionale di Fisica Nucleare; the Ministry of Education, Culture, Sports, Science and Technology of Japan; the Natural Sciences and Engineering Research Council of Canada; the National Science Council of the Republic of China; the Swiss National Science Foundation; the A.P. Sloan Foundation; the Bundesministerium fuer Bildung und Forschung, Germany; the Korean Science and Engineering Foundation and the Korean Research Foundation; the

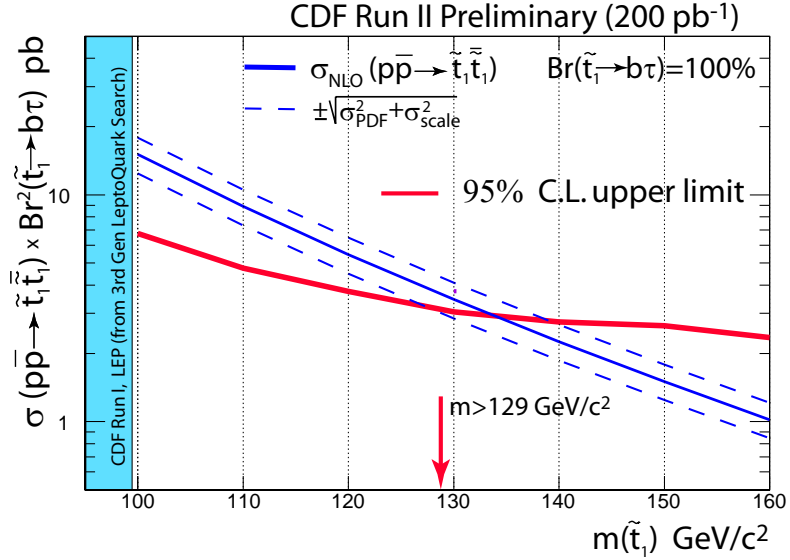


FIG. 3: 95% C.L. limit curve for the  $\tilde{t}_1\tilde{t}_1$  production cross section (thick solid line) with the NLO calculations (solid line) for the cross section [12]. The uncertainties of the theoretical calculation due to choice of PDFs and normalization scales are also shown (dashed lines). Previous constraint obtained from CDF and LEP leptoquark searches ( $m(\tilde{t}_1) > 99 \text{ GeV}/c^2$ ) is also shown.

Particle Physics and Astronomy Research Council and the Royal Society, UK; the Russian Foundation for Basic Research; the Comision Interministerial de Ciencia y Tecnologia, Spain; and in part by the European Community's Human Potential Programme under contract HPRN-CT-2002-00292, Probe for New Physics.

- 
- [1] H.P. Nilles, Phys. Rep. **110**, 1 (1984); H.E. Haber and G.L. Kane, *ibid.* **117**, 75 (1985). For recent review on SUSY, see S.P. Martin, "A Supersymmetry Primer," hep-ph/9709356.
- [2] K. Inoue, A. Kakuo, H. Komatsu, and H. Takeshita, Prog. Theor. Phys **68**, 927 (1982); *ibid.* **71**, 413 (1984); L. Ibanez and C. Lopez, Nucl. Phys. B **233**, 511 (1984); J. Ellis and S. Rudaz, Phys. Lett. B **128**, 248 (1983).
- [3] S. Weinberg, Phys. Rev. D **26**, 287 (1982); G. Farrar and S. Weinberg, *ibid.* **27**, 2732 (1983); S. Dawson, Nucl. Phys. B **261**, 297 (1985). For recent reviews on  $R_p$  violating SUSY, see H. Dreiner, hep-ph/9707435; F. de Campos *et al.*, hep-ph/9903245.
- [4] CDF II Collaboration, FERMILAB-PUB-96/390-E.
- [5] A. Anastassov *et al.*, Nucl. Instrum. Methods Phys. Res. Sect. A **518**, 609 (2004).
- [6] We use a coordinate system where  $\theta$  and  $\phi$  are the polar and azimuthal angles, respectively, with respect to the proton beam direction ( $z$  axis). The pseudorapidity  $\eta$  is defined as  $-\ln[\tan(\theta/2)]$ . The transverse momentum of a particle is denoted as  $p_T = p \sin \theta$ . The analogous quantity using energies, defined as  $E_T = E \sin \theta$ , is called transverse energy. The missing transverse energy,  $\cancel{E}_T$ , is a magnitude of  $\vec{\cancel{E}}_T \equiv -\sum E_T^i \hat{n}_i$ , where  $\hat{n}_i$  is the unit vector in the transverse plane pointing from the interaction point to the energy deposition in calorimeter cell  $i$ .
- [7] The charged particle tracking system is enclosed in a superconducting magnet and consists of multi-layer silicon detectors and a large open-cell drift chamber (COT) covering  $|\eta| < 1$ . The calorimeter system is organized into electromagnetic (EM) and hadronic (HAD) sections segmented in projective tower geometry, covering  $|\eta| < 3.6$ . The central muon detection system is located outside of the calorimeter, used for this analysis, covering  $|\eta| < 1$ . The relevant detector sub-systems for this analysis are the central electromagnetic (CEM) calorimeter, central muon (CMUP) detector, and central muon extension (CMX) detector, the COT system, and the trigger system for tracks in COT (XFT).
- [8] CDF Collaboration, D. Acosta *et al.*, Phys. Rev. Lett. **92**, 051803 (2004).
- [9] T. Sjöstrand *et al.*, Comput. Phys. Commun. **135**, 238 (2001). We use PYTHIA version 6.216.
- [10] R. Brun *et al.*, CERN-DD/EE/81-1 (1987).
- [11] CTEQ Collaboration, H.L. Lai *et al.*, Eur. Phys. J. C **12**, 375 (2000).
- [12] W. Beenakker, R. Höpker, M. Spira, and P. M. Zerwas, Nucl. Phys. B **492**, 51 (1997). We use PROSPINO version 2.